Nanoscale

PAPER

View Article Online
View Journal

Cite this: DOI: 10.1039/c7nr05446g

Electroconductive nanoscale topography for enhanced neuronal differentiation and electrophysiological maturation of human neural stem cells†

Kisuk Yang,[a] Seung Jung Yu,[b] Jong Seung Lee,[a] Hak-Rae Lee,[b] Gyeong-Eon Chang,[a] Jungmok Seo,[c] Taeyoon Lee,[d] Eunji Cheong,*[a] Sung Gap Im *[b] and Seung-Woo Cho *[a,e]

Received 25th July 2017,
Accepted 12th November 2017

DOI: 10.1039/c7nr05446g

rsc.li/nanoscale

Biophysical cues, such as topography, and electrical cues can provide external stimulation for the promotion of stem cell neurogenesis. Here, we demonstrate an electroconductive surface nanotopography for enhancing neuronal differentiation and the functional maturation of human neural stem cells (hNSCs). The electroconductive nanopatterned substrates were prepared by depositing a thin layer of titanium (Ti) with nanograting topographies (150 to 300 nm groove/ridge, the thickness of the groove – 150 μm) onto polymer surfaces. The Ti-coated nanopatterned substrate (TNS) induced cellular alignment along the groove pattern *via* contact guidance and promoted focal adhesion and cytoskeletal reorganization, which ultimately led to enhanced neuronal differentiation and maturation of hNSCs as indicated by significantly elevated neurite extension and the upregulated expression of the neuronal markers Tuj1 and NeuN compared with the Ti-coated flat substrate (TFS) and the nanopatterned substrate (NS) without Ti coating. Mechanosensitive cellular events, such as β1-integrin binding/clustering and myosin–actin interaction, and the Rho-associated protein kinase (ROCK) and mitogen-activated protein kinase/extracellular signal regulated kinase (MEK-ERK) pathways, were found to be associated with enhanced focal adhesion and neuronal differentiation of hNSCs by the TNS. Among the neuronal subtypes, differentiation into dopaminergic and glutamatergic neurons was promoted on the TNS. Importantly, the TNS increased the induction rate of neuron-like cells exhibiting electrophysiological properties from hNSCs. Finally, the application of pulsed electrical stimulation to the TNS further enhanced neuronal differentiation of hNSCs due probably to calcium channel activation, indicating a combined effect of topographical and electrical cues on stem cell neurogenesis, which postulates the novelty of our current study. The present work suggests that an electroconductive nanopatterned substrate can serve as an effective culture platform for deriving highly mature, functional neuronal lineage cells from stem cells.

Introduction

Biophysical cues that mimic the nanotopography features of native extracellular matrices have been of great importance in the regulation of diverse cellular behaviors including survival, adhesion, proliferation, differentiation, and migration.[1–6] Stem cells can interact with topographical cues in many ways, often through a naturally occurring process known as contact guidance, which is characterized by cellular responses to nano- and micro-scale structures.[7–9] It is also known that topographical cues modulate stem cell–substrate interactions through the control of integrin binding.[1,10] Further, contact guidance and integrin control by topographical cues reportedly change the cellular alignment and integrin clustering, which subsequently activates focal adhesion assembly, actin remodeling, and

[a]Department of Biotechnology, Yonsei University, Seoul 03722, Republic of Korea. E-mail: seungwoocho@yonsei.ac.kr, eunjicheong@yonsei.ac.kr
[b]Department of Chemical and Biomolecular Engineering and Graphene Research Center in KI for NanoCentury, Korea Advanced Institute of Science and Technology, Daejeon 34141, Republic of Korea. E-mail: sgim@kaist.ac.kr
[c]Center for Biomaterials, Korea Institute of Science and Technology, Seoul 02792, Republic of Korea
[d]School of Electrical and Electronic Engineering, Yonsei University, Seoul 03722, Republic of Korea
[e]Center for Nanomedicine, Institute for Basic Science (IBS), Seoul 03722, Republic of Korea

†Electronic supplementary information (ESI) available. See DOI: 10.1039/c7nr05446g

nuclear deformation signaling processes.[10–12] Therefore, topographical cues can initiate mechanosensitive cascades for the signaling pathways that affect stem cell differentiation.[10,12–14] Indeed, several reports have elucidated the functional roles of nano- and micro-patterned topographies in directing stem cell differentiation towards neuronal lineages.[10,12,14–16] However, the current strategies that entail patterned structures need to be upgraded for the generation of highly mature, functional neuron-like cells because simple topographical cues alone are often insufficient to direct the functional maturation of differentiated stem cells during neurogenesis.[12,17]

Electrical stimulation might provide another effective cue for stem cells that could be combined with topographical cues to induce the functional neuronal differentiation of stem cells. It is well known that bioelectricity plays an important role in the development, maturation, and biological functions of the nervous systems.[18,19] Several neural tissue-engineering studies have developed polymer substrates and scaffolds with an electroconductive polymer or metal deposits that could provide stem or progenitor cells with electrical stimulation for the enhancement of neuronal differentiation.[20–23] For example, electrical stimulation using an electroconductive polymer (polypyrrole) dramatically increased neurite formation and the extension of neural cells.[24] Electrically-stimulated neural cells on the polypyrrole-deposited nanofiber scaffolds exhibited enhanced neurite outgrowth compared to non-stimulated cells. In another study, electrically conductive carbon nanotube substrates that provided electrical stimulation to neural stem cells (NSCs) during culture significantly promoted the outgrowth of neurites and their differentiation into mature neurons.[25] Interestingly, Yang *et al.* recently reported on electroconductive patterned substrates for the enhanced myogenic differentiation and maturation of myoblasts.[26]

In this study, we report on an electroconductive substrate with geometrically well-defined nanotopography for enhancing neuronal differentiation and the electrophysiological maturation of human NSCs (hNSCs), even in the absence of supplementation with neurotrophic soluble factors. The nanopatterned polyurethane-acrylate (PUA) substrates were prepared by capillary force lithography (CFL),[26] which was followed by the deposition of a thin layer of titanium (Ti) onto the substrates using an electron-beam evaporator. Ti was selected as the conductive coating due to its excellent electroconductivity and biocompatibility.[27] The Ti-coated nanopatterned substrate (TNS) simultaneously provides both topographical cues and the electrical environment to synergistically promote neuronal differentiation and the functional maturation of hNSCs. Importantly, the application of a pulsed electrical current to the electroconductive nanopatterned substrates further promotes neuronal differentiation of hNSCs, indicating a combined effect of biophysical and electrical cues on hNSC neurogenesis. Accordingly, our study suggests the utility of electroconductive nanotopography for the production of neuronal cells exhibiting functionally mature neuronal phenotypes from human stem cells.

Experimental

Fabrication and characterization of electroconductive nanopatterned substrates

Polyurethane-acrylate (PUA; MINS 311 RM, Minuta Technology Co., Ltd, Gyeonggi, Korea) substrates were prepared using CFL techniques as previously reported.[26] Briefly, two drops of PUA resin were poured onto a nanopatterned silicon (Si) master mold that had been generated using standard photolithography and covered with a poly(ethylene terephthalate) (PET) film (Skyrol®, SKC Co., Ltd, Seoul, Korea). The PUA resin was then cured in an ultraviolet (UV) cure system (~365 nm; Minuta Technology Co., Ltd, Gyeonggi, Korea) by exposure to UV light at 20 mW cm^{-2} for 10 seconds. The PET film with the PUA resin was then peeled off from the Si master mold. The nanopatterned PUA resin on the PET film was then further exposed to UV light for 24 hours for complete curing. The nanopatterned PUA substrates were then soaked in isopropyl alcohol for 30 minutes and then in distilled water for 30 minutes for cleaning.

For the electroconductive coating, titanium (Ti) was deposited on the PUA nanopatterned substrates as previously reported.[26] Briefly, the base pressure of the evaporator was maintained at 7.0×10^{-6} Torr. The Ti tablets (Thifine, Incheon, Korea) were placed on the electron-beam source and film thickness was monitored *in situ* using a quartz crystal thickness monitor. The final thickness of the Ti on the PUA nanopatterned substrates was 30 nm at a deposition rate of 1.0 Å s^{-1}.

For surface characterization, the topography and morphology of fabricated patterned substrates were observed by scanning electron microscopy (SEM; FEI Sirion SEM, Hillsboro, OR, USA) and atomic force microscopy (AFM; PSIA XE-100 AFM, Santa Clara, CA, USA) as previously described.[26]

Electrical conductivity measurement

For the hNSC culture, fibronectin (FN) was coated onto the fabricated nanopatterned substrates to facilitate cell adhesion. The electrical conductivity (σ, S cm^{-1}) of Ti-coated nanopatterned substrate (TNS) with or without FN coating ($n = 3$) was then measured according to our previous protocol[28] using a four-point probe with a dual configuration method and a sheet resistance meter (FPP-2400, Dasol Eng., Cheongju, Korea); the values of each substrate were compared.

hNSC culture

The expansion of undifferentiated human neural stem cells (hNSCs) was performed as previously described.[10] hNSCs were isolated from human fetal telencephalic tissue at 13 weeks of gestation. hNSCs were kindly provided from Prof. Kook In Park at Yonsei University College of Medicine. Before hNSC seeding, the substrates were cleaned with 70% ethanol for 1 hour and coated with FN by simple immersion in a 10 μg ml^{-1} FN solution (Sigma-Aldrich, St Louis, MO, USA) for 2 hours. For spontaneous differentiation, hNSCs that dissociated from the neurospheres were seeded onto the substrates

at a seeding density of 4.5×10^4 cells per cm^2 and maintained in culture conditions without supplementation with basic fibroblast growth factor (bFGF) and leukemia inhibitory factor (LIF).[10] For cell viability test after 2 days of culture, the mitochondrial metabolic activities of hNSCs were determined with 3-[4,5-dimethylthiazol-2-yl]-2,5 diphenyl tetrazolium bromide (MTT) assay (Sigma-Aldrich). The cells received electrical stimulation the next day after cell seeding and the MTT test was conducted one day later. The viability of hNSCs was determined by measuring the optical absorbance of each sample at 595 nm using a microplate reader (Infinite M200 Pro, Tecan, Maennedorf, Switzerland) and normalizing the value of each group to that of the hNSCs on FS.

Immunocytochemistry

Immunocytochemistry staining was conducted as previously reported.[29] The following primary antibodies were used for the staining: mouse monoclonal anti-neuronal class III β-tubulin (Tuj1) (1 : 100; Millipore, Temecula, CA, USA), rabbit polyclonal anti-microtubule-associated protein 2 (MAP2) (1 : 200; Santa Cruz Biotechnology, Santa Cruz, CA, USA), mouse monoclonal anti-Nestin (1 : 200; Milipore), rabbit polyclonal anti-glial fibrillary acidic protein (GFAP) (1 : 200; Millipore), rabbit polyclonal anti-neuronal specific nuclear protein (NeuN) (1 : 200; Millipore), mouse monoclonal anti-glutamic acid decarboxylase (GAD67) (1 : 200; Abcam, Cambridge, UK), rabbit polyclonal anti-glutamate transporter (GluT) (1 : 200; Abcam), and rabbit polyclonal anti-tyrosine hydroxylase (TH) (1 : 200; Cell Signaling Technology, Beverly, MA, USA). The following secondary antibodies were used: Alexa Fluor®488 goat anti-mouse IgG (1 : 500; Invitrogen, Carlsbad, CA, USA) and Alexa Fluor®594 donkey anti-rabbit IgG (1 : 500; Invitrogen). Counterstaining of the cell nuclei was conducted with 4′,6-diamidino-2-phenylindole (DAPI, Sigma-Aldrich). The fluorescently stained signals were detected under a confocal microscope (LSM 700, Carl Zeiss, Jena, Germany). Neurite formation and cell body length were measured from Tuj1-stained cell images as previously described.[12] Neurite formation was quantified as the percentage ratio of Tuj1-positive cells with extended neurites to total cells (DAPI-positive cells). Focal adhesion and cytoskeleton staining (vinculin and filamentous actin; F-actin) was performed with the Actin Cytoskeleton and Focal Adhesion Staining Kit (FAK100, Millipore).

Gene expression analysis

Quantitative real-time polymerase chain reaction (qPCR) analysis was performed as previously described.[30] Briefly, TaqMan® Gene Expression Assay (Applied Biosystems, Foster City, CA, USA) was used to measure gene expression in hNSCs on the substrates for each target (Tuj1, Hs00801390_s1; GFAP, Hs00909238_g1; GluT, Hs00220404_m1; GAD67, Hs01065893_m1; TH, Hs00165941_m1; focal adhesion kinase (FAK), Hs01056457_m1; vinculin, Hs00419715_m1; MAP2, Hs00258900_m1; Oct4, Hs00742896_s1; Nanog, Hs02387400_g1; Nes, Hs00707120_s1; voltage-gated sodium channel alpha subunit 1 (SCN1α), Hs00374696_m1; and calcium channel, voltage-dependent, L type, alpha 1C subunit (CACNA1C), Hs00167681_m1). Gene expression in each group was determined using the comparative C_t method and by normalizing the expression of each target gene to that of an endogenous reference transcript (glyceraldehyde 3-phosphate dehydrogenase (GAPDH), Hs02758991_g1).[17]

Western blot

Western blot assays were performed as previously described.[12] The primary antibodies used were as follows: rabbit polyclonal anti-phosphorylated focal adhesion kinase (pFAK) (pY397, 1 : 1000; Invitrogen), rabbit polyclonal anti-FAK (1 : 1000; Cell Signaling Technology), rabbit polyclonal anti-phosphorylated extracellular-regulated kinase 1/2 (ERK1/2) (pERK1/2, 1 : 000; Cell Signaling Technology), rabbit monoclonal anti-GAPDH (1 : 4000; Cell Signaling Technology), and rabbit polyclonal anti-β-actin (1 : 2000; Cell Signaling Technology). The target protein signals were detected using a Clarity™ Western ECL Substrate (Bio-Rad, Hercules, CA, USA) according to the manufacturer's instructions. The individual experiments for western blot analysis were performed three times (n = 3) with 4 samples in each analysis.

Inhibition studies

Inhibition studies for various cellular events and pathways were performed as previously described.[31] The following inhibitors were used to treat hNSCs upon cell seeding: anti-β1 integrin (1 : 40 dilution; Millipore), 50 μM blebbistatin (Sigma-Aldrich), 25 μM U0126 (MEK1/2 inhibitor, Cell Signaling Technology), and 10 μM Y27632 (Rho-associated protein kinase (ROCK) inhibitor, Millipore). The β1 integrin neutralizing antibodies (Milipore, CP26) were used to block hNSC adhesion *via* β1 integrin.

Electrophysiology

The electrophysiological analysis was conducted as previously described.[12] Whole-cell patch clamping for measuring the action potential and ion channel current of hNSCs that differentiated on the substrates was performed after 5 days in culture. The cells for recording neural signals in our patch clamp setting were continuously superfused with artificial cerebrospinal fluid (aCSF) containing 124 mM NaCl, 3 mM KCl, 1.3 mM $MgSO_4$, 1.25 mM NaH_2PO_4, 26 mM $NaHCO_3$, 2.4 mM $CaCl_2$–$2H_2O$, and 10 mM glucose.[12,31,32] This solution was continuously aerated by O_2 95%/CO_2 5% mixed gas at room temperature. Whole cell patch clamping was conducted by using glass capillary pipet tips filled with internal pipet solution. Internal pipet solution contains 115 mM K-gluconate, 10 mM KCl, 10 mM HEPES, 10 mM EGTA, 5 mM Mg-ATP, and 0.5 mM Na^{2+}-GTP, with pH 7.3 and 280–285 mOsm.[12,31,32] The cells were treated with tetrodotoxin (TTX, 0.5 μM; Sigma-Aldrich) for 5 minutes to determine whether the currents and spikes were specific to the sodium channel.

Electrical stimulation

Starting 1 day after hNSC seeding on the PUA substrates with or without nanopatterns (NS and FS) and the TNS, cells were electrically stimulated using a programmable digital power supply (MK3003P, MK Power, Seoul, Korea). Pulsed electrical stimulation (1 Hz, 30 min, twice a day) was directly applied to the TNS through the wires connecting TNS to power supply (Fig. S1†). The contact for electricity supply was made to the substrates by fixing the wires with poly(dimethylsiloxane) (PDMS) on both sides of the TNS. The electrical current was applied in the parallel direction to the grating axis of the TNS. The maximum current and voltage were limited to 3 μA and 25 V, respectively. After 5 days in culture, the expression of differentiation markers (*Tuj1*, *MAP2*, and *GFAP*) and calcium ion channel (*CACNA1C*) in the hNSCs was quantified by qPCR analysis. For calcium imaging analysis after 5 days of culture, hNSCs on the TNS were stained with Fluo-4 AM dye (Invitrogen) before electrical stimulation. Time-lapse changes in calcium influx level in hNSCs were imaged using a confocal microscope (LSM 700, Carl Zeiss) under electrical stimulation.

Statistical analysis

Statistical analyses were conducted with an unpaired Student's *t*-test using Sigma-Plot software (Systat Software Inc., Chicago, IL, USA) as previously described.[32] Values of $p < 0.01$ or 0.05 were considered statistically significant.

Results and discussion

Fabrication and characterization of TNS

The CFL method was utilized for fabricating nanopatterned substrates (Fig. 1). The PUA resin was dispensed onto a Si master mold covered with a PET film and exposed UV light for curing (Fig. 1). The cured PUA resin with the PET film overlay was then detached from the Si master mold and further exposed to UV light for complete curing. Finally, the fabricated PUA nanopatterned substrates were coated with Ti at a thickness of 30 nm using an electron-beam evaporator and subsequently used for hNSC culture (Fig. 1). We chose Ti for electroconductive coating since Ti has excellent biocompatibility, high strength, and electrical conductivity, and thus it has been widely utilized for various medical implants and devices including bone implants, stents, heart valves, and hearing aids.[33–36] To investigate its surface morphology, the fabricated TNS was analyzed by AFM and SEM (Fig. 2A and B). The AFM analysis revealed that all of the fabricated nanopatterned substrates uniformly displayed well-defined ridge/groove structures on their surfaces (Fig. 2A). The SEM images of the substrates demonstrated that Ti deposition *via* electron-beam evaporation covered the perimeter of the grooved nanopatterns and did not significantly alter the original topographies (Fig. 2B). The sizes of the prepared ridge/groove patterned TNS structures (height, 300 nm) were 150, 200, 250, and 300 nm, respectively. Finally, the TNS was coated with FN to facilitate cell adhesion on the surfaces before cell seeding. Compared to pristine TNS, the FN coating was found to decrease the electrical conductivity of the Ti-coated patterned surfaces (bare TNS, 1250 ± 68 S cm^{-1} *versus* FN-modified TNS, 916 ± 23 S cm^{-1}; Fig. 2C), but the conductivity value appeared to remain effective for generating electrical stimulation to the cells.[24] The coating of extracellular matrix proteins such as collagen and FN forms a thin layer on the surface[37] and often reduces the conductivity of electroconductive materials deposited on the surface. For example, Akkouch *et al.* reported that the coating of FN on the polypyrrole decreased the conductivity of polypyrrole.[38] They also demonstrated that the decrease of conduc-

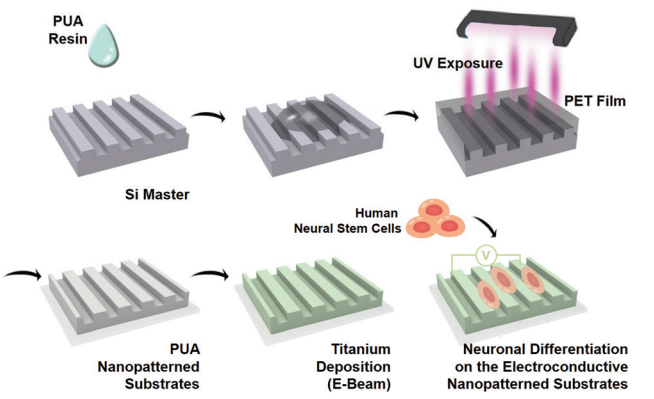

Fig. 1 Schematic illustration of the fabrication of electroconductive nanopatterned substrates for the enhancement of hNSC neuronal differentiation.

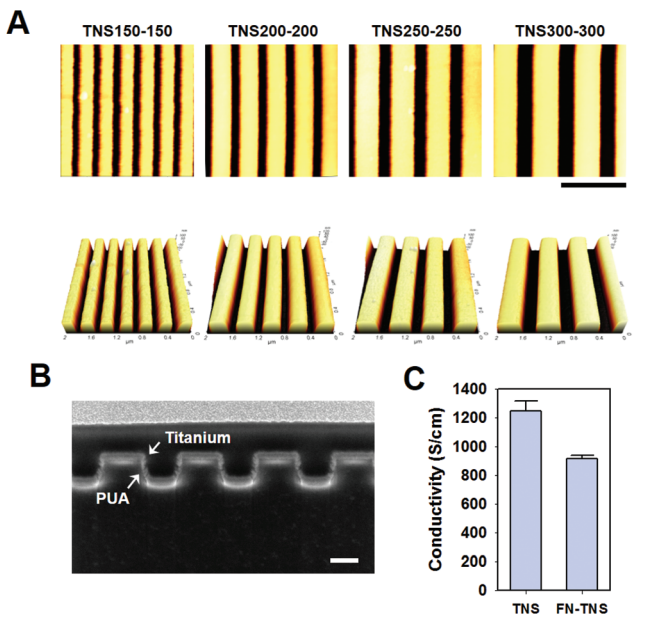

Fig. 2 Surface characterization of the Ti-coated nanopatterned substrate (TNS). (A) AFM analysis of the substrates with groove/ridge sizes ranging from 150 to 300 nm, scale bar = 1 μm. (B) SEM image of TNS with 150–150 nm groove/ridge patterns, scale bar = 100 nm. (C) The electrical conductivity of TNS (150–150 nm groove/ridge) with or without a fibronectin (FN) coating.

tivity by protein coating was more evident with FN than with bovine serum albumin protein and was apparently dependent upon FN dose. Therefore, FN coating in our study may reduce somewhat the conductivity of Ti substrate. The conductivity value of PUA substrate without Ti coating is zero, indicating its non-conductive property.

Enhancement of hNSC neuronal differentiation by TNS

The modification of nanotopography with an electroconductive coating significantly enhanced neuronal differentiation of hNSCs derived from human fetal brain under mitogenic factor-free culture conditions, allowing for spontaneous differentiation. Five days after the culture of hNSCs on the substrates, immunofluorescence staining of hNSCs for neuronal (Tuj1) and astrocytic (GFAP) lineage markers indicated that the culture of hNSC on the TNS with groove sizes of 150 nm and 200 nm resulted in an increased number of Tuj1-positive cells and a decreased number of GFAP-positive cells (Fig. 3A). Accordingly, the proportion of Tuj1-positive neuronal lineage cells in the total population was much greater on the TNS with 150 nm and 200 nm-sized groove patterns than on the Ti-coated flat substrate (TFS), whereas the population of GFAP-positive astrocytic lineage cells was comparatively lower on the TNS than on the TFS (Fig. 3B). hNSCs cultured on the TNS exhibited greater neurite formation and body length compared to the TFS group (Fig. 3C). *Tuj1* expression was significantly upregulated in the hNSCs that differentiated on the TNS, especially on the TNS with 150 and 200 nm-sized grooves (Fig. 3D). A quantitative real-time polymerase chain reaction (qPCR) data for *GFAP* expression in TNS groups with different dimensions of groove nanopattern showed that there was no significant difference in *GFAP* expression among the groups (Fig. 3D). After 12 days of differentiation, the neuronal cells that differentiated from hNSCs on the TNS with a 150 nm groove exhibited substantially enhanced expression of NeuN, a mature neuronal marker, compared to the cells that differentiated on the TFS (Fig. 3E). A qPCR data revealed that the expression of *NeuN* was significantly enhanced ($p < 0.01$) in hNSCs cultured on TNS compared to cells on TFS (Fig. 3F). In addition, the proportion of NeuN-positive cells also increased

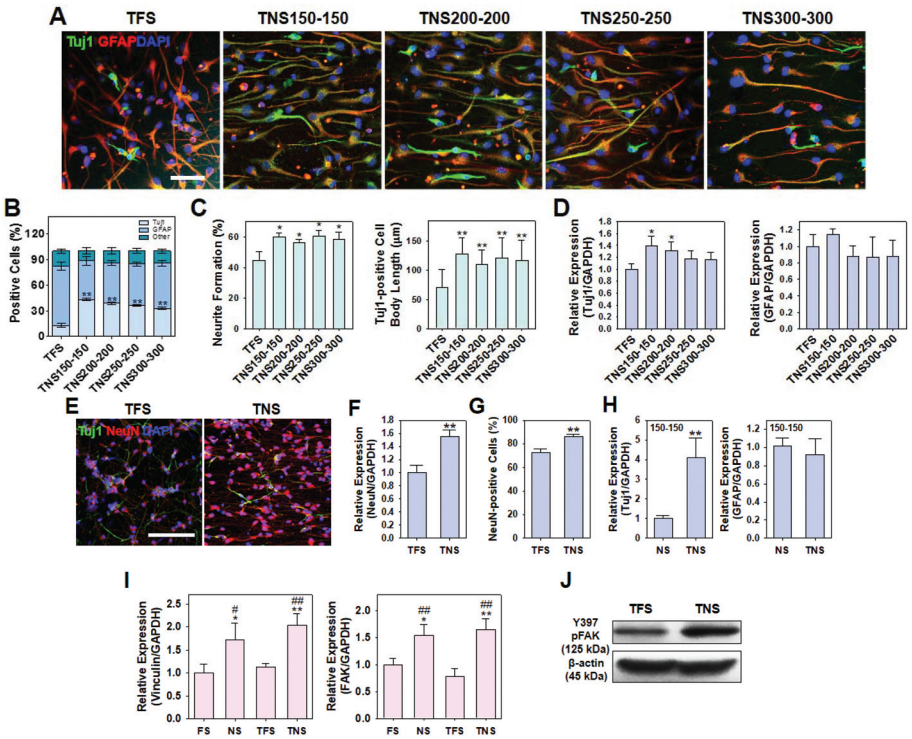

Fig. 3 Enhanced neuronal differentiation and focal adhesion signal activation of hNSCs on TNS. (A) Immunofluorescent staining of hNSCs that differentiated into neuronal (Tuj1) and astrocytic (GFAP) lineages on the substrates after 5 days; scale bar = 50 μm. (B) The relative proportion of Tuj1- or GFAP-positive cells on the substrates ($n = 4$; $^{**}p < 0.01$ *vs.* TFS group). (C) Quantification of neurite formation ($n = 3$) and body length ($n = 15$) of Tuj1-positive cells ($^{*}p < 0.05$, $^{**}p < 0.01$ *vs.* TFS group). qPCR analysis of the expression of the neuronal marker (D) *Tuj1* and *GFAP* in hNSCs grown on the substrates for 5 days ($n = 3$; $^{*}p < 0.05$ *vs.* TFS group). (E) Immunofluorescence analysis of the neuronal markers Tuj1 and NeuN was performed with hNSCs that differentiated on the substrates (TFS and TNS with 150–150 nm groove patterns for 12 days; scale bar = 100 μm). (F) qPCR analysis of the expression of *NeuN* in hNSCs grown on TFS and TNS (150–150 nm) for 12 days ($n = 3$, $^{**}p < 0.01$ *vs.* TFS group). (G) The relative proportion of NeuN-positive cells on the substrates ($n = 3$; $^{**}p < 0.01$ *vs.* TFS group). (H) qPCR analysis of the expression of *Tuj1* and the astrocyte marker *GFAP* in hNSCs grown on NS (150–150 nm) and TNS (150–150 nm) for 5 days ($n = 3$; $^{**}p < 0.01$ *vs.* NS group). (I) qPCR analysis to examine the expression of focal adhesion protein genes (*VCL* and *FAK*) in hNSCs grown on each substrate for 5 days ($n = 3$; $^{*}p < 0.05$, $^{**}p < 0.01$ *vs.* FS group, $\#p < 0.05$, $\#\#p < 0.01$ *vs.* TFS group). (J) Western blotting was conducted to compare the expression of phosphorylated FAK [pFAK(Y397)] in hNSCs cultured on TFS and TNS (150–150 nm).

($p < 0.01$) on the TNS group (86.2 ± 1.5%) compared to TFS group (72.6 ± 3.1%), indicating the promoted differentiation of hNSCs to mature neuronal lineage by the TNS (Fig. 3G). These results indicate that TNS could enhance neuronal differentiation of hNSCs and further direct hNSC differentiation to a neuronal lineage rather than to an astrocytic lineage.

The thickness of the groove patterns is sure to be an important parameter for regulating stem cell differentiation. Actually, the aspect ratio (depth/width) of topographical features has been shown to affect diverse cellular behaviors including stem cell differentiation.[9,39] For example, it was shown that neurite elongation, alignment, and neuronal differentiation of murine neural progenitor cells were promoted as the increase in grating depth.[9] In another study, Crouch *et al.* fabricated micro- and nanoscale gratings or their combinations in polystyrene plates to investigate anisotropic behaviors of human dermal fibroblasts with respect to the aspect ratio of gratings and confirmed that both cell alignment and elongation increased with an increase in the aspect ratio.[39] In the current study, we did not examine the effect of nanopatterned groove thickness on hNSC differentiation. Thus, we should carefully investigate the effect of different grating thickness on hNSC behaviors including focal adhesion, neurite extension, and differentiation in the future studies.

We also examined if the electrical conductivity generated by the Ti-coating promotes the neuronal differentiation of hNSCs. A qPCR analysis revealed that *Tuj1* expression was highly enhanced (4-fold higher) in the hNSCs cultured on TNS with 150 nm grooves/ridges, compared with the cells cultured on nanopatterned substrate with the same patterned structures without Ti coating (NS group) (Fig. 3H). Interestingly, the expression of the astrocyte marker *GFAP* was not significantly different between the TNS and NS groups (Fig. 3H). These qPCR data indicate that the electroconductive Ti coating was specifically effective at directing the differentiation of hNSCs to a neuronal lineage. Previous studies have also demonstrated the effectiveness of Ti-modified patterned surfaces for muscular and vascular cell maturation.[26,40] It was found that skeletal myoblasts grown on a Ti-grafted topographical surface exhibited increased expression of myogenic marker genes, indicating that the substrate topography and conductivity could play a synergistic role in the engineering of functional skeletal muscle tissue.[26] Likewise, Ti-patterned substrates improve endothelial functions by inducing a highly aligned native cellular morphology.[40] Cellot *et al.* reported that electroconductive nanostructured surfaces can improve the propagation of action potential in hippocampal neurons *via* forming tight contacts between carbon nanotube surfaces and cell membranes and inducing calcium channel clustering.[41] Passive stimulation by electroconductive substrates could provide the beneficial effects on hNSC neurogenesis. Several studies have demonstrated that inherent electroconductivity of the substrates could promote neurogenesis of stem cells by forming tight contact between cell membranes and substrate surfaces to favor electrical shortcuts in neural cells[41–43] even in the absence of active electrical stimulation. Similarly, in our current study, we showed that electroconductive Ti coating itself can enhance neuronal differentiation of hNSCs even without pulsed electrical stimulation, indicating passive stimulation of substrate electroconductivity on hNSC neurogenesis. Ti coating may also facilitate FN adsorption on the substrate, increase the mass of FN, and enhance exposure of the adhesion domain of FN,[44] influencing neuronal differentiation of hNSCs in combination with topographical cues. Overall, we confirmed that a combination of nanotopography and electroconductive stimulation could lead to a marked promotion of hNSC neuronal differentiation.

The enhanced neuronal differentiation of hNSCs by TNS originated from both the development of focal adhesions activated by nanotopography and the electrical cues from the electroconductive Ti coating. Previous studies, including ours, have demonstrated that topographical stimulation by micro- and nanopatterned surfaces can promote NSC differentiation *via* the assembly of focal adhesion-related proteins including vinculin, paxillin, and FAK.[3,8,10,12,17,45] In our previous study, we also showed that nanopatterned substrates with small size of groove patterns can provide more contact points that facilitate focal adhesion formation in hNSCs than flat substrates or substrates with larger size of submicron groove patterned structures, leading to enhanced neuronal differentiation of hNSCs.[10] Since nanopatterned substrates with smaller size of groove width can facilitate integrin clustering, they may be able to induce highly compact focal adhesion clusters.[46,47] In the present study, a qPCR analysis to examine the effect of non-conductive NP substrates on cytoskeletal and adhesion behaviors of hNSCs indicated that non-conductive NS and TNS groups showed higher expression level of vinculin and FAK than FS and TFS groups (Fig. 3I), indicating that nanotopography may be more critical for focal adhesion formation than electroconductivity. Western blot analysis of FAK phosphorylation in hNSCs revealed that the expression of pFAK was highly upregulated in hNSCs grown on TNS compared with the cells grown on TFS (Fig. 3J), which indicates the activation of FAK signaling by nanotopography cues.

Actually, several studies have reported that phosphorylation of FAK or paxillin induces strong focal adhesion turnover and disassembly of focal adhesion in migrating cells.[48,49] The study described by Hamadi *et al.* has reported the involvement of p397 FAK in the disassembly of focal adhesion during migration of human astrocytoma cells. Another study reported by Zaidel-Bar *et al.* demonstrated that phosphorylation of paxillin regulates both the assembly and turnover of focal adhesion. They showed that phosphorylated paxillin enhanced lamellipodial protrusions, whereas non-phosphorylated paxillin was critical for fibrillar adhesion formation. There have been more studies demonstrating correlation of small point contacts with a strong focal adhesion turnover in neurons, particularly in the growth cone,[50–53] and the effect of integrin clustering-restricting nanostructures on neuritogenesis.[54] However, there have also been several studies reporting other roles of phosphorylation of FAK or paxillin in focal adhesion regulation,[5,55–61] which are rather controversial to previous

studies mentioned above. In addition, several studies employing nanopatterned structures, especially groove nanopatterns, have demonstrated that nanopatterned groove structures with smaller size induce better focal adhesion development and are more effective for promoting stem cell differentiation than groove nano- or submicron-patterns with larger size,[16,46,47,62–64] which are consistent with the findings in our current study. The discrepancy between these literatures on focal adhesion development may be due to different experimental cell conditions (*e.g.*, migrating condition *versus* adhesive condition), the use of different types of nanostructures (*e.g.*, assembled nanoparticles *versus* groove nanopatterns), and different pattern scales (*e.g.*, submicron-scale *versus* nano-scale). Although we observed that pFAK phosphorylation and focal adhesion development were facilitated by TNS, we need to more carefully investigate this phenomenon under various experimental conditions in the future studies.

In our current study, we utilized nanopatterned substrates for electroconductive surface fabrication, but electrospinning-based alternative platforms could also be applied for the fabrication of highly effective electroconductive substrates. Electrospun nanofibrous scaffolds have been extensively used for neural tissue engineering due to several advantages including large surface area and highly fibrous microenvironment for cell loading and mass transfer.[65] Micro- and nano-patterning of electrospun nanofibrous membranes could also provide robust culture platforms for improving neurogenesis.[66] Thus, electrospun nanofiber-based substrates modified with electroconductive polymers or metals would become robust engineering platforms to improve stem cell neurogenesis by maximizing the synergistic effects of biophysical and electrical cues.

Mechanotransduction mechanisms for enhanced neuronal differentiation of hNSCs by TNS

In this study, we confirmed that TNS contributes to the enhanced neuronal differentiation of hNSCs *via* a series of cellular events associated with mechanosensitive signal transduction. As shown in Fig. 4A (no treatment groups; TFS *versus* TNS with 150 nm groove), TNS facilitated the alignment of the hNSC cytoskeleton (F-actin) and significantly promoted the formation of hNSC focal adhesion. The hNSCs cultured on TNS exhibited a highly extended, elongated alignment of F-actin filaments along the grooved nanopatterns (Fig. 4A). In contrast, the elongated alignment of F-actin filaments was not observed in hNSCs cultured on TFS and the hNSC F-actin filaments were randomly oriented on TFS (Fig. 4A). Immunofluorescence staining of hNSCs for vinculin, one of the major focal adhesion proteins, showed that hNSC focal adhesion formation was significantly stimulated on TNS compared to TFS without nanotopography (Fig. 4A). The quantitative data of the density of vinculin-positive cells on each substrate indicated larger number of vinculin-positive cells in TNS group than in TFS group (Fig. 4B). Our previous study demonstrated that nanopatterned substrates with groove and pillar structures with the range of several hundred nanometers may be able to provide more contact points that facilitate focal adhesion formation of hNSCs than flat surface without nanopatterns since they could mimic the topographies produced by extracellular matrices optimal for focal adhesion development and maturation.[10] It is known that alteration in focal adhesion formation and cytoskeletal reorganization in stem cells is involved in mechanotransduction signaling for the control of stem cell differentiation.[58,67]

Several critical cellular processes and pathways have been suggested to explain the potential mechanisms of topographical cues involved in focal adhesion development and enhanced neuronal differentiation in hNSCs. Mechanotransduction signaling is generally initiated by the recognition of substrate surface topographical cues *via* integrin-mediated binding; thus, we first targeted integrin binding as a starting point for the regulation of focal adhesion development, the FAK pathway, and differentiation of hNSCs.[5,68] Because TNS was coated with FN to promote hNSC adhesion, the adhesion of hNSCs to the TNS *via* FN was blocked using antibodies against β1 integrin, an integrin subtype that mediates cell binding to FN (Fig. 4A). Treatment with β1 integrin antibodies significantly inhibited vinculin-positive focal adhesion assembly in the hNSCs cultured on TNS (Fig. 4A). Likewise, the expression of focal adhesion proteins FAK and vinculin in the hNSCs cultured on TNS was significantly downregulated following treatment with β1 integrin antibodies (Fig. 4C), which subsequently led to a significant decrease in the gene and protein expression of Tuj1 and GFAP (Fig. 4D and E). Treatment of β1 integrin antibodies may affect directly adhesion of hNSCs, leading to decreased hNSC differentiation including glial lineage since integrin-mediated adhesion of the cells is critical for initiating differentiation process.[69,70] This result strongly suggests that β1 integrin-mediated adhesion of hNSCs onto the nanotopography features is critical for focal adhesion development and stem cell differentiation.

Next, we identified several other pathways associated with the effects of TNS on enhanced focal adhesion formation and differentiation of hNSCs by conducting inhibition studies. For the inhibition experiments, hNSCs were plated onto the substrates and treated with inhibitors of cytoskeletal contractility, blebbistatin, an inhibitor of myosin II, and Y27632, an inhibitor of ROCK pathway. hNSCs were also treated with an inhibitor of differentiation-related signal transduction, U0126, which is an inhibitor MEK1/2. In general, treatment with these inhibitors interrupted hNSC adhesion and alignment, reduced focal adhesion formation (Fig. 4A), and consequently caused a significant decrease in the differentiation of hNSCs into neuronal lineage (Fig. 4E). qPCR analysis of the focal adhesion markers *FAK*, *VCL* (vinculin), and differentiation markers *Tuj1*, *GFAP* indicated that their expression levels in hNSCs upregulated by the TNS with 150 nm groove patterns were significantly hindered by treatment with these inhibitors (Fig. 4C and E). MEK1/2 pathway is known to be involved in stem cell differentiation including glial lineage as well as neuronal lineage,[71–73] and thus U0126 treatment to block MEK1/2 pathway may also reduce the expression of GFAP in hNSCs on TFS and TNS.

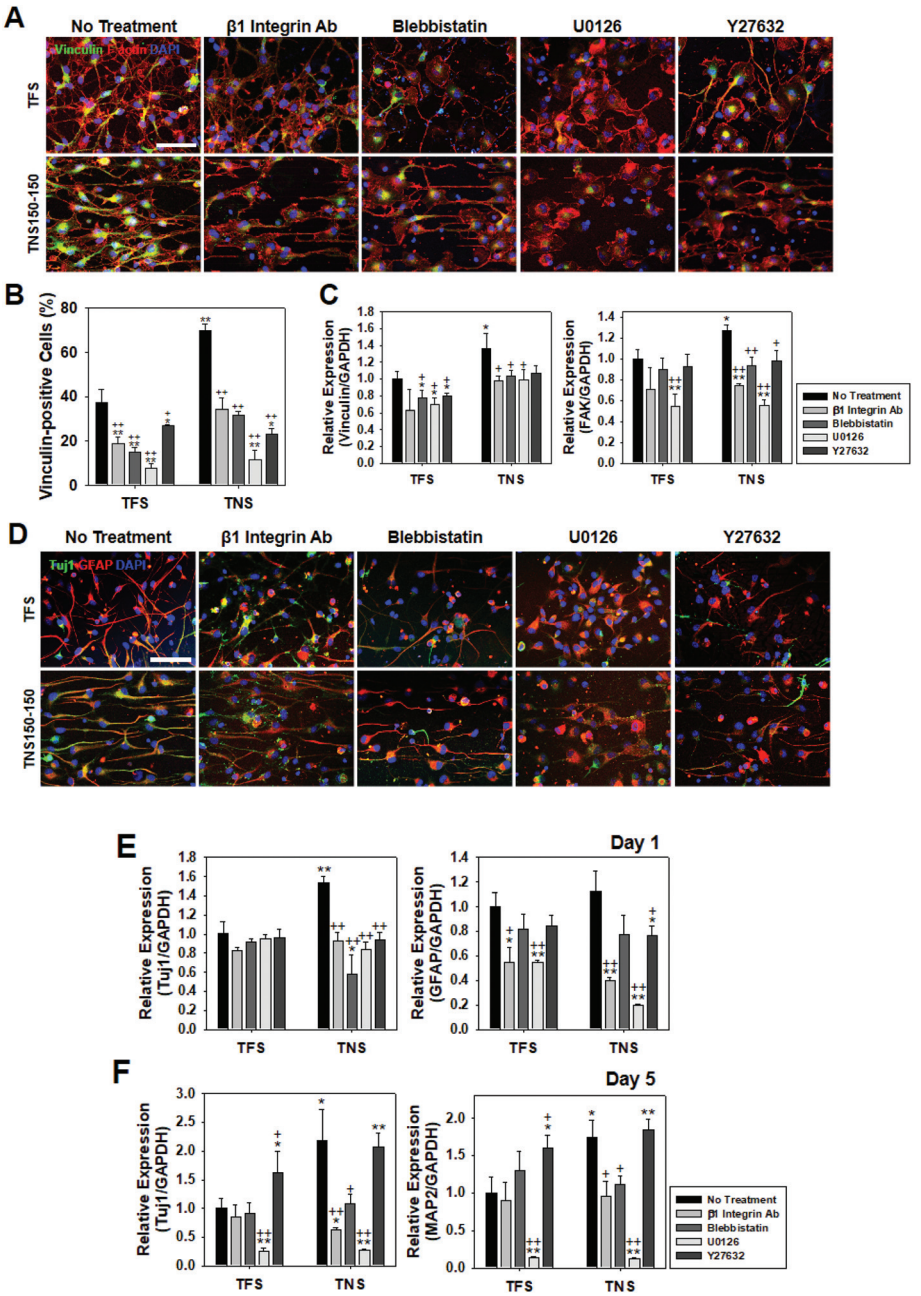

Fig. 4 Inhibition studies to reveal potential mechanisms of enhanced neuronal differentiation by TNS. To block integrin binding and mechanotransduction-associated signals, hNSCs were plated with β1 integrin antibodies, blebbistatin (myosin II inhibitor), U0126 (MEK1/2 inhibitor), and Y27632 (ROCK inhibitor). (A) Immunofluorescence analysis was performed for focal adhesion (vinculin) and cytoskeleton (F-actin) proteins using hNSCs cultured on TFS and TNS (150–150 nm) with or without the treatments; scale bar = 50 μm. Counterstaining with DAPI was conducted to stain cell nuclei. (B) Quantification of vinculin-positive cells from the vinculin-stained images (n = 3, *p < 0.05, **p < 0.01 *vs.* No treatment in TFS group, +p < 0.05, ++p < 0.01 *vs.* No treatment in each substrate). (C) qPCR analysis was conducted to investigate the expression of *VCL* and *FAK* in hNSCs cultured on TFS and TNS (150–150 nm) with or without the treatments (n = 3, *p < 0.05, **p < 0.01 *vs.* no treatment in TFS group, +p < 0.05, ++p < 0.01 *vs.* no treatment in each substrate). (D) Immunofluorescence analysis was performed for differentiation markers (Tuj1 and GFAP) using hNSCs cultured on TFS and TNS (150–150 nm) with or without the treatments; scale bar = 50 μm. Counterstaining with DAPI was conducted to stain cell nuclei. qPCR analysis was conducted to investigate the expression of (E) *Tuj1* and *GFAP* (1 day in culture) or (F) *Tuj1* and *MAP2* (5 days in culture) in hNSCs cultured on TFS and TNS (150–150 nm) with or without the treatments (n = 3, *p < 0.05, **p < 0.01 *vs.* no treatment in TFS group, +p < 0.05, ++p < 0.01 *vs.* no treatment in each substrate).

Our results from chemical inhibitor treatment studies demonstrate that actin organization and actomyosin contractility induced by TNS were also critical for the enhanced neuronal differentiation and neuronal maturation of hNSCs. The ROCK pathway is one of the major cytoskeleton regulators.[57,74] Because ROCK activation modulates cytoskeletal organization,

cellular contractility, and cell migration by inducing the formation of actin stress fibers and focal contacts, and also by increasing the activity of the motor protein myosin II,[74,75] we assumed that the ROCK pathway was a major transducer of mechanical signals from the TNS.[57] As expected, the treatment with Y27632, an inhibitor of the ROCK pathway, significantly decreased F-actin alignment, vinculin-associated focal adhesion assembly, and ultimately the neuronal differentiation of hNSCs on TNS (Fig. 4).[76] Inhibition of myosin II, which is responsible for actomyosin contractility, by treatment with blebbistatin similarly dissipated the alignment of F-actin along the patterned structures and downregulated the expression of focal adhesion proteins and differentiation markers in the cells grown on the TNS (Fig. 4). Together, these results demonstrate the importance of cytoskeletal organization and actomyosin contractility induced by surface topographical cues in regulating focal adhesion formation and differentiation in stem cells. In fact, Ankam *et al.* reported that actomyosin contractility plays a critical role in MAP2 expression during nanotopography-directed neuronal differentiation of human embryonic stem cells.[77] The U0126 treatment-mediated inhibition of the mitogen-activated protein kinase/extracellular signal regulated kinase (MEK-ERK) pathway, which is reportedly associated with the topography cue-mediated mechanotransduction signaling cascades for enhancing stem cell differentiation,[55,78] completely reversed the effect of TNS on promoting neuronal differentiation of hNSCs (Fig. 4). Therefore, the results from our inhibition studies demonstrate that TNS-mediated enhancement of neuronal differentiation in hNSCs might also be due to the activation of signaling pathways associated with neuronal differentiation, such as MEK-ERK, following mechanosensitive cellular processes including integrin binding and clustering, actin rearrangement, actomyosin contractility induction, and FAK-mediated focal adhesion assembly.[10]

However, several studies have shown that the treatment of inhibitors for ROCK pathway (Y27632) and actomyosin contractility (blebbistatin) enhanced neuronal differentiation of stem cells.[79–82] In our current study, there was no significant difference in the gene expression of Tuj1 in hNSCs between inhibitor-treated TFS groups and non-treated TFS groups 1 day after treatment of inhibitors (Fig. 4E). On the other hand, the treatment of these inhibitors to hNSCs on the TNS downregulated the gene expression of Tuj1 in hNSCs compared to no inhibitor treatments (Fig. 4E). Similarly, other group also reported that both blebbistatin and Y27632 inhibited the upregulation of MAP2 (mature neuronal marker) by topography in the stem cells.[58] Although our data showed that Tuj1 expression upregulated by TNS was reversed by inhibitor treatments, we monitored the differentiation at relatively early time point (~1 day). In addition, considering no significant difference in the Tuj1 expression of TFS groups with or without inhibitors, inhibition of ROCK pathway and actomyosin contractility seems to reverse Tuj1 expression increased by nanotopography to the level of non-treated cells rather than reducing neuronal differentiation of hNSCs. Thus, to check more accurately the effect of such inhibitor treatments on the differentiation capacity of hNSCs on each substrate, the gene expression of neuronal markers (*Tuj1*, *MAP2*) in the hNSCs on the substrates was examined at longer time point (5 days after the treatment of inhibitors) (Fig. 4F). A qPCR data to check the differentiation of hNSCs 5 days after inhibitor treatments showed that blebbistatin treatment did not increase neuronal differentiation of hNSCs on both TFS and TNS, but the treatment of Y27632 increased the expression of *Tuj1* and *MAP2* in hNSCs particularly on the TFS, compared with no treatment (Fig. 4F). Therefore, we may conclude that inhibition of ROCK and actomyosin contractility did not induce further enhancement in neuronal differentiation of hNSCs on TNS probably due to the significant effect of nanotopography, but could contribute to promoting hNSC neurogenesis on TFS without topographical stimulation. Of course, these issues should be more precisely investigated in the future work.

Guided differentiation of hNSCs into specific neuronal subtypes by TNS

The combined effects of nanotopography and electroconductive stimulation on guiding the differentiation of hNSCs into more specialized neuronal subtypes, such as glutamatergic neurons, GABAergic neurons, and dopaminergic neurons, were tested. Previous reports indicate that topographical cues affect neuronal specification and differentiation propensity during the differentiation of NSCs.[10,12,17,83] Electrical stimulation has also been shown to influence the differentiation of stem cells into specific neuronal subtypes.[18] Immunocytochemistry staining for specific neuronal subtype markers, including glutamatergic neuron marker (GluT), GABAergic neuron marker (GAD67), and dopaminergic neuron marker (TH), revealed that TNS guided the differentiation of hNSCs to GABAergic and dopaminergic neuronal lineages rather than to a glutamatergic neuronal lineage (Fig. 5A). The relative percentage ratio of GAD67-positive cells to GluT-positive cells increased on the TNS compared to other substrates (FS, NS, and TFS) (Fig. 5B). qPCR analysis also revealed that *GAD67* and *TH* expression increased, whereas *GluT* expression decreased, in hNSCs grown on TNS compared with the cells cultured on other substrates (FS, NS, and TFS groups; Fig. 5C–E). These data demonstrate that the combination of topographical and electrical cues could guide hNSC differentiation into inhibitory neurons (*e.g.*, GABAergic neurons) rather than into excitatory neurons (*e.g.*, glutamatergic neurons).[84] TNS also directed differentiation of hNSCs into dopaminergic neuronal lineage (Fig. 5E), reflecting the feasibility of TNS as a culture platform to produce cell therapeutics for the treatment of Parkinson's disease.

Neuronal subtype specification of stem cells is of great importance for therapeutic applications and neurological disease models because imbalance of excitatory and inhibitory neurons is known to be often associated with occurrence of neuronal disorders.[85,86] In particular, several diseases such as Huntington's disease, schizophrenia, autism, and epilepsy are caused by the loss and defects of inhibitory neurons.

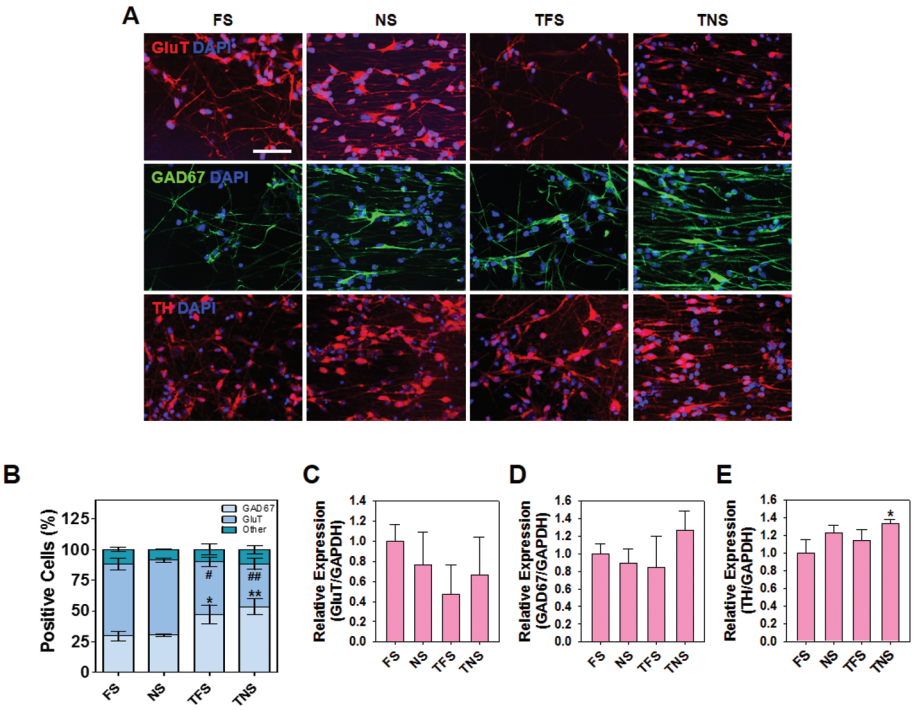

Fig. 5 Neuronal differentiation of hNSC subtypes guided by TNS. (A) Immunofluorescence staining of hNSCs for neuronal subtype markers (GluT, glutamatergic neuron; GAD67, GABAergic neuron; and TH, dopaminergic neuron) following differentiation on the substrates after 12 days in culture; scale bar = 50 μm. The TNS with 150–150 nm groove patterns was used for the experiments. (B) The relative proportion of GAD67 or GluT-positive cells on the substrates (n = 3; *p < 0.05, **p < 0.01 *vs.* GAD67-positive cells in FS group, #p < 0.05, ##p < 0.01 *vs.* GluT-positive cells in FS group). qPCR analysis to examine the expression of neuronal subtype marker genes (C) *GluT*, (D) *GAD67*, and (E) *TH* in hNSCs cultured on the substrates for 12 days (n = 3; *p < 0.05 *vs.* FS group).

Therefore, the population ratio between GABAergic neuron and glutamatergic neuron would be obviously relevant to normal and pathological neural conditions. In our current study, we confirmed that the culture of hNSCs on the TNS facilitates hNSC differentiation to inhibitory neuronal lineage (*e.g.*, GABAergic neuron) rather than to excitatory neuronal lineage (*e.g.*, glutamatergic neuron) (Fig. 5B). Therefore, TNS may be able to provide cell therapeutics to treat neuronal disorders caused by the loss and defects of inhibitory neurons.

Improved electrophysiological properties of functional neuron-like cells from hNSCs on TNS

A whole-cell patch clamping analysis was conducted to compare the electrophysiological properties of differentiated hNSCs grown on TNS and TFS (Fig. 6). The neuron-like cells that differentiated from hNSCs on TNS exhibited large inward cation currents, presumably conducted by voltage-gated sodium channels (Fig. 6A), and thus generated action potentials (Fig. 6B), which are considered essential features of functional neurons (Fig. 6A and B). To verify the channel subtypes that mediated currents and spikes, TTX, an antagonist for voltage-gated sodium channels, was applied to the cells. The sodium channels were blocked by TTX treatment, and action potentials and sodium currents consequently disappeared (Fig. 6A and B after TTX). These results support the notion that currents and spikes in the differentiated hNSCs on TNS

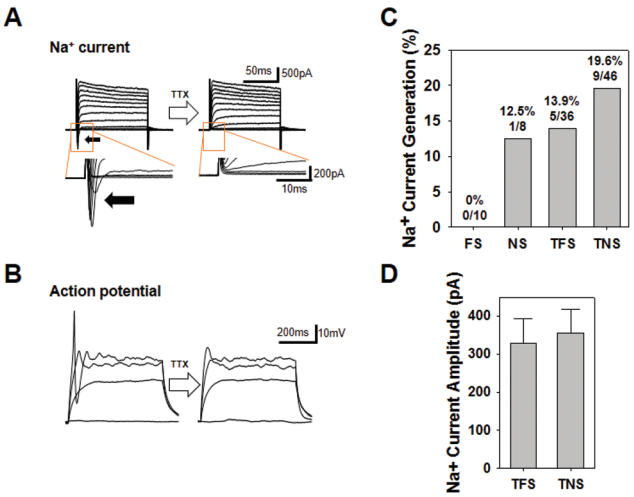

Fig. 6 Electrophysiological analysis of hNSCs differentiated on TNS for 5 days. Electrophysiological analysis was conducted for the recording of (A) sodium channel currents and (B) action potential from hNSCs differentiated on TNS (150–150 nm). The currents and action potential spikes disappeared after TTX treatment (sodium channel blocker). Comparison of (C) population of cells generating sodium currents and (D) average amplitude of sodium currents between the TNS and TFS groups. The number seen in patch clamp analysis data indicates the number of cells showing sodium current firing spikes/the number of the cells examined with whole cell patch clamp.

were mainly mediated by voltage-gated sodium channels. More importantly, the percentage of sodium current-generating cells in the total cells examined by patch clamp analysis was higher in the TNS group than in the TFS group (TNS, 19.6% *versus* TFS, 13.9%; Fig. 6C), suggesting that a combination of nanotopography and electroconductive cues could increase the efficiency of deriving functional neuron-like cells from hNSCs. The average sodium current amplitude of the TNS group was slightly greater than that of the TFS group, but the difference was not statistically significant (Fig. 6D).

Pulsed electrical stimulation for further promoting neuronal differentiation of hNSCs

Finally, we examined whether neuronal differentiation of hNSCs on the TNS could be further promoted by applying pulsed electrical stimulation to the cells during culture on TNS. To this end, TNS was connected in a series and a single-phase pulse was applied to the substrates to conduct electrical stimulation to the hNSCs (1 Hz, 30 min twice a day; Fig. 7A). The maximum applied current and voltage were limited to 3 μA and 25 V, respectively, to protect the cells from damage due to excess electrical stimulation (Fig. 7A). The electrical stimulation by our protocol did not reduce the mitochondrial metabolic activity of hNSCs on the substrates due to the application of electrical parameters (the maximum current of 3 μA and voltage of 25 V) previously optimized for cell stimulation (Fig. S2†). In our previous study reporting development of a novel electrical stimulation platform to accelerate direct neuronal conversion and neuronal maturation,[87] we optimized electrical stimulation parameters and identified these particular values which do not affect cell viability but increase neuronal transdifferentiation.

Double immunofluorescent staining for MAP2/GFAP after 5 days in culture and quantification data of the relative population of neuronal (MAP2-positive) and astrocytic (GFAP-positive) lineage cells revealed that the percentage of MAP2-positive cells increased by nanotopography, Ti electroconductive coating, and pulsed electrical stimulation (Fig. 7B and C). MAP2-positive cell population was the highest in the ETNS group with combined topographical and electrical stimulations (56.2 ± 1.3%) than other control groups (FS group; 24.6 ± 2.0%, NS group; 37.1 ± 2.1%, TFS group; 40.6 ± 0.7%, TNS group; 48.4 ± 2.1%, ETFS group; 48.9 ± 2.6%) (Fig. 7C). A qPCR analysis to confirm the differentiation of hNSCs was performed after 5 days in culture with electrical stimulation. qPCR data revealed that the expression of *Tuj1* and *MAP2* was markedly upregulated in hNSCs cultured on TNS or TFS with pulsed electrical stimulation (ETNS, ETFS) compared to those on TNS or TFS with no electrical stimulation (TNS, TFS; Fig. 7D). Interestingly, the electrical stimulation did not increase the expression of *GFAP* in hNSCs on the TNS or TFS (Fig. 7E), indicating that the astrocytic differentiation of hNSCs is not affected by electrical stimulation. Electrical stimulation did not affect the expression of stem cell markers (*Nestin*, *Oct4*, *Nanog*) (Fig. 7F). Together, our data demonstrate that electroconductive nanotopography with pulsed electrical stimulation can accelerate neuronal differentiation of stem cells but does not support astrocytic differentiation and proliferation of hNSCs. The quantification data of the intensity ratio of Y397 pFAK band to total FAK or β-actin band from western blot analysis of the hNSCs after 5 days of culture indicated that the cells on the TNS either with or without electrical stimulation (TNS, ETNS) showed higher levels of the pFAK/FAK or pFAK/β-actin ratio than the cells on the TFS without nanopatterns (TFS, ETFS) (Fig. 7G and H).

Our results clearly demonstrate that several biophysical cues such as electroconductive coating (T), nanotopography (N), and electrical stimulation (E) significantly enhance neuronal differentiation of hNSCs individually or in combination. Electrophysiological analysis of hNSCs differentiated under culture conditions without E, T, and N did not show sodium current generation within 5 days in culture, indicating that hNSC differentiation takes much longer in the absence of these biophysical factors. In previous studies, micro- and nanoscale groove patterned substrates were reported to induce about 1.5-fold increase in MAP2 expression[16] and 2.4–2.8-fold increase in Tuj1 expression compared to flat substrate.[8,88] In our study, qPCR analysis confirmed that the ETNS increased *Tuj1* and *MAP2* expression by 2–2.5 fold compared with FS (Fig. 7D). Although the increase in neurogenesis of hNSCs by ETNS seems to be similar level to that by previously reported patterned substrates, considering the difference in stem cell types, analytical methods, and time points for the analysis between our study and others, nanotopography with electrical stimulation (ETNS) might be more effective for neuronal differentiation and maturation of hNSCs than the existing methods. Interestingly, the effect of electrical stimulation on enhancing neuronal differentiation of hNSCs was more significant on the TFS than on the TNS (TFS *versus* ETFS and TNS *versus* ETNS; Fig. 7D). The population of MAP2-positive cells quantified from MAP2-stained images was greater in ETNS group (56.2 ± 1.3%) than in ETFS group (48.9 ± 2.6%) (Fig. 7C), but there was no significant difference ($p < 0.05$) in the gene expression of Tuj1 and MAP2 between ETFS and ETNS groups as shown in qPCR analysis (Fig. 7D). Therefore, although electroconductive Ti coating and topographical stimulation can promote neurogenesis of hNSCs, the effect of these factors may be overridden by the electrical stimulation. This indicates that active electrical stimulation may be more critical parameter for stem cell neurogenesis than other biophysical factors, which needs to be further examined in future work.

Electrical cues might be able to enhance hNSC neurogenesis *via* specific ion channel activation. Here, we confirmed that the expression of *CACNA1C* voltage-gated calcium channel and *SCN1α* voltage-gated sodium channel increased in hNSCs grown on ETNS compared to the cells grown on TNS with no electrical stimulation (Fig. 8A). Our qPCR data demonstrated that the expression of neuronal markers (*Tuj1*, *MAP2*) and ion channels (*SCN1α*, *CACNA1C*) increased by nanotopography and electroconductive Ti coating, and further increased by active electrical stimulation (Fig. 7D and 8A). Our previous study revealed that electrical stimulation created by a triboelectric

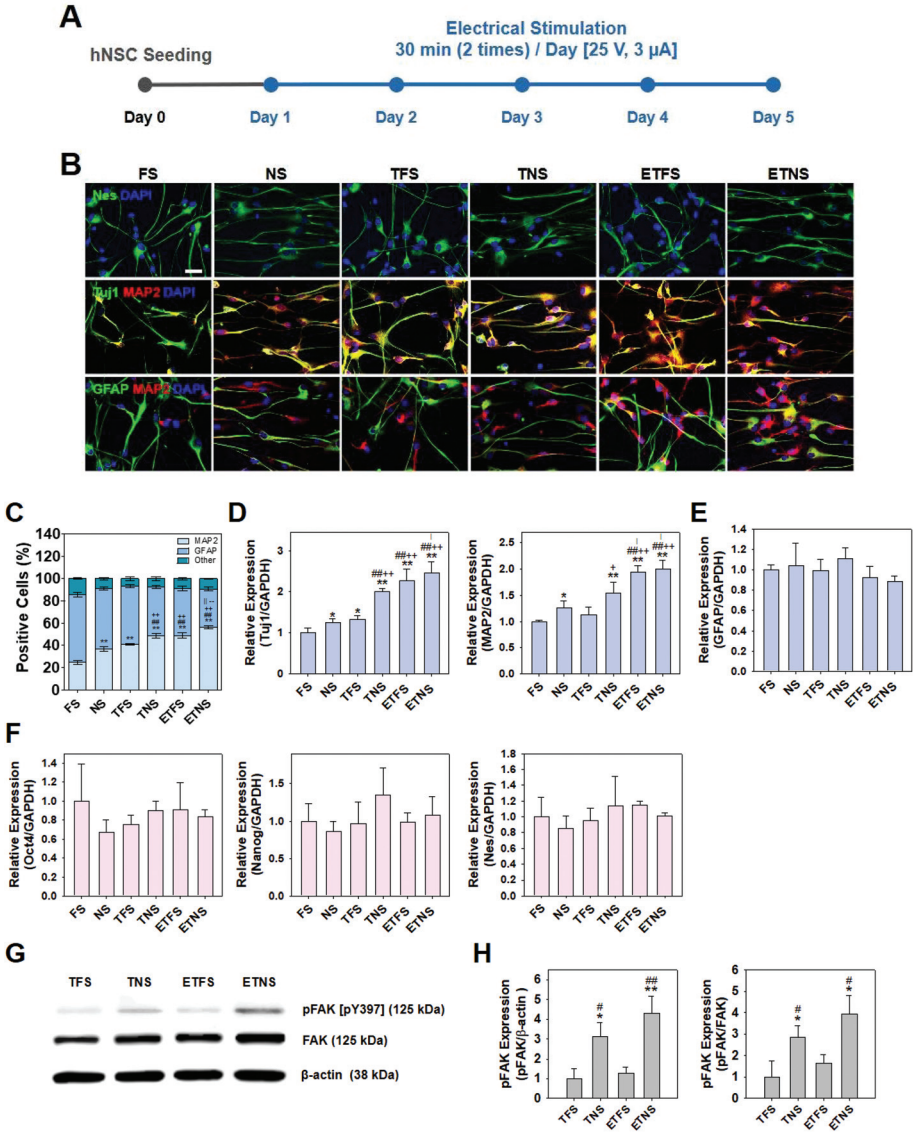

Fig. 7 Electrical stimulation for improving neuronal differentiation of hNSCs on TNS. (A) The protocol for pulsed electrical stimulation of hNSCs cultured on the substrates. Starting 1 day after hNSC seeding on the TNS (150–150 nm), the cells were electrically stimulated with 25 V and 3 μA for 30 minutes twice a day (ETNS). Differentiation of hNSCs on the substrates after 5 days in culture. (B) Immunofluorescent staining of hNSCs differentiated on each substrate for neuronal (Tuj1 and MAP2), astrocyte (GFAP), and undifferentiated NSC (Nestin) markers, scale bar = 50 μm. (C) The relative proportion of MAP2- or GFAP-positive cells on the substrates (n = 3, $^{**}p < 0.01$ *vs.* FS group, $\#\#p < 0.01$ *vs.* NS group, $++p < 0.01$ *vs.* TFS group, $||p < 0.01$ *vs.* TNS group, $--p < 0.01$ *vs.* ETFS group). qPCR analysis was conducted to examine the expression of (D) neuronal markers (*Tuj1* and *MAP2*), (E) astrocytic lineage marker (*GFAP*), and (F) self-renewal markers (*Oct4*, *Nanog* and *Nes*) in hNSCs (n = 3, $^{*}p < 0.05$, $^{**}p < 0.01$ *vs.* FS group, $\#\#p < 0.01$ *vs.* NS group, $+p < 0.05$, $++p < 0.01$ *vs.* TFS group, $|p < 0.05$ *vs.* TNS group). (G) Western blot analysis of phosphorylated FAK [pFAK (Y397)] protein expression in hNSCs grown on each substrate after 5 days in culture. β-Actin and total FAK were used as loading controls for the comparison of pFAK(Y397) protein expression. (H) Quantitative analysis of pFAK/β-actin and pFAK/FAK in each group (n = 3, $^{*}p < 0.05$, $^{**}p < 0.01$ *vs.* TFS group, $\#p < 0.05$, $\#\#p < 0.01$ *vs.* ETFS group).

nanogenerator activates voltage-gated calcium channels, increases calcium ion influx, and promotes ERK1/2 phosphorylation, which is known to affect neuronal differentiation.[87] Consequently, a series of these cellular events following the activation of calcium channels by electrical stimulation enhanced the neuronal transdifferentiation of primary mouse embryonic fibroblasts to induced mature neurons.[87] Therefore, pulsed electrical stimulation applied to the TNS could also enhance the functional neuronal maturation of hNSCs through the activation of calcium channels and other subsequent signaling cascades in accord with our previous observations. Calcium influx imaging of hNSCs on the TNS using calcium indicator, Fluo-4 AM, indicated increased intracellular calcium influx into hNSCs and membrane depolarization upon electrical stimulation (Fig. 8B). Western blot data showed increased phosphorylation of ERK1/2 (pERK1/2) in hNSCs on

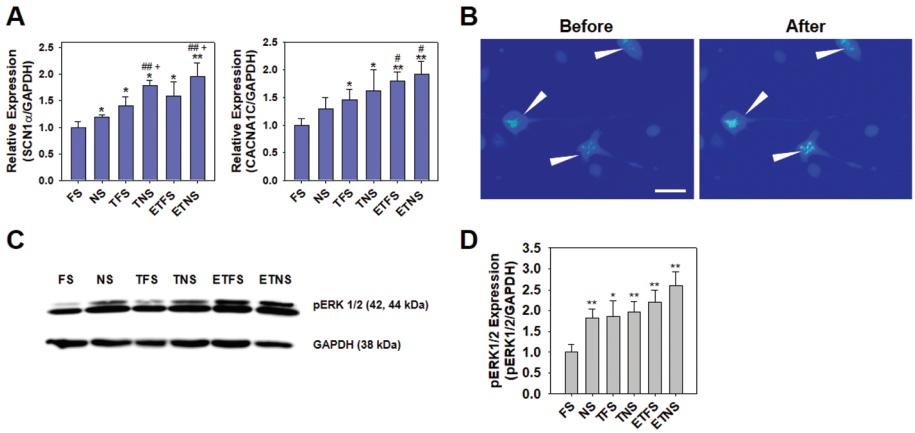

Fig. 8 Activation of ion channels, depolarization, and downstream signaling pathway in hNSCs on TNS with electrical stimulation. (A) qPCR analysis to examine the expression of voltage-gated sodium channel (*SCN1α*) and voltage-gated calcium channel (*CACNA1C*) in hNSCs grown on the substrates after 5 days in culture ($n = 3$, $^{*}p < 0.05$, $^{**}p < 0.01$ *vs.* FS group, $\#p < 0.05$, $\#\#p < 0.01$ *vs.* NS group, $+p < 0.05$ *vs.* TFS group). (B) Calcium imaging of Fluo-4 AM-treated hNSCs on the TNS during exposure to electrical stimulation. White arrowheads indicate the increase in fluorescent signals from Fluo-4 AM, scale bar = 20 μm. (C) Western blot analysis of phosphorylated ERK1/2 (pERK1/2) expression in hNSCs on each substrate after 5 days in culture. (D) Quantitative analysis of pERK1/2 expression relative to GAPDH expression in each group ($n = 3$, $^{*}p < 0.05$, $^{**}p < 0.01$ *vs.* FS group).

the TNS with electrical stimulation (ETNS group) (Fig. 8C and D). Thus, we speculate that electrical stimulation of electroconductive TNS activates voltage-gated ion channels and sequentially promotes ERK1/2 phosphorylation of hNSCs on the TNS, leading to enhanced hNSC neurogenesis. These data may suggest a novel finding of our current study to elucidate the roles of combined topographical cue and electrical stimulation on stem cell neurogenesis.

Prior reports have indicated that the application of electrical stimulation promotes the neuronal differentiation of stem cells. A previous study performed by Stewart *et al.* indicated that electrical stimulation of the conductive polymer polypyrrole predominantly induced differentiation of hNSCs to Tuj1-expressing neurons, whereas the induction of GFAP-expressing glial cells was lower,[89] which is consistent with our current electrical stimulation study findings showing the differentiation propensity of electrically-stimulated hNSCs towards a neuronal lineage (Fig. 7C). The prior study showed that the electrically-stimulated cells displayed neuronal phenotypes with longer neurites and increased branching compared to unstimulated cells.[89] Yamada *et al.* also demonstrated that mild electrical stimulation induced embryonic stem cells to differentiate specifically into neuronal lineage cells *via* the induction of a calcium ion influx.[18] More interestingly, the electrically-stimulated embryonic stem cells contributed to the formation of neurons within an injured spinal cord, whereas unstimulated stem cells formed few neurons in the tissue.[18] In another study which employed similar methods and parameters for electrical stimulation to our current study,[90] Balikov *et al.* reported that electrical stimulation through wires connected to the graphene-based micropatterned substrates with similar protocols to ours enhances neuronal development of human mesenchymal stem cells *in vitro*, which is also consistent with the results from our current study. Although previous literature suggests implications of electrical stimulation on stem cell differentiation, to the best of our knowledge, our current study is the first to entail stimulation through the combined application of topographical and electrical cues for the promotion of the neuronal differentiation of human stem cells, which postulates the novelty of our current study. Nonetheless, the long-term effects of electrical stimulation and additional details regarding the mechanisms underlying enhanced neuronal differentiation need to be further elucidated in future studies.

Conclusions

Here, we demonstrate the effectiveness of electroconductive nanotopography for promoting neuronal differentiation and the functional maturation of hNSCs. Further, we confirmed that the nanotopography features generated on the substrates enhanced functional neuronal differentiation of hNSCs *via* mechanotransduction cascades including integrin clustering, cytoskeletal (F-actin and myosin) reorganization, and the ROCK and MEK/ERK downstream signaling pathways. Interestingly, the subtype specification of hNSCs into inhibitory neuronal lineage cells and the derivation of electrophysiologically active neuronal cells from hNSCs were promoted on the electroconductive TNS. The pulsed electrical stimulation applied to the electroconductive TNS further enhanced neuronal differentiation of hNSCs *via* combined effects of the topographical and electrical cues. Accordingly, our study might further encourage the application of electroconductive materials modified with various biophysical cues for the induction of desirable stem cell phenotypes and acceleration of neural tissue regeneration.

Our current study has a novelty in terms of experimental design and biological outcomes; (1) in this study we employed a combination strategy of topographical and electrical stimu-

lation based on TNS for hNSC differentiation. We provided the cells with real active electricity not just passive stimulation by electroconductive Ti coating and proved the effect of electrical cues on stem cell differentiation, (2) we also revealed that besides mechanotransduction pathways activated by nanotopography, ion channel expression and membrane depolarization activated by electrical stimulation contributed to enhanced neurogenesis of hNSCs, which may suggest the potential mechanisms and novel findings to elucidate the effect of active electrical cues on stem cell behaviors. Considering that previous studies have mostly employed topographies with simple patterned structures for stem cell differentiation and have rarely provided the evaluation of differentiated stem cells in terms of electrophysiological functionality and ion channel activation, our current study may have benefits in experimental design for stem cell differentiation and biological outcomes by combined topographical and electrical stimulations.

We think that electroconductive substrates with nanotopographical features could serve as platforms to produce functional cell therapeutics exhibiting mature neuronal phenotypes, functionalities, and in turn improved therapeutic efficacy for the treatment of neurodegenerative diseases and neuronal disorders. Of course, through more elaborative work in the future study, our systems should be scaled up to enable mass production of a larger amount of functional neuron-like cells, and the fidelity and robustness of the systems to ensure reproducible cell therapeutic efficacy should be achieved through further improvement of nanofabrication techniques and electroconductive material modification.

Conflicts of interest

There are no conflicts to declare.

Acknowledgements

This work was supported by grants (2015R1A2A1A15053771, 2016M3C9A4921712, and 2017M3C7A1023471) from the National Research Foundation of Korea (NRF), the Ministry of Science and ICT (MSIT), Republic of Korea. This work was also supported by the Advanced Biomass R&D Center (ABC) of Global Frontier Project funded by the Ministry of Science and ICT (MSIT) (ABC-2010-0029728). This work was also supported by the Institute for Basic Science (IBS-R026-D1) and the Yonsei University Future-Leading Research Initiative of 2016 (2016-22-0102). This work was supported by International Collaborative R&D Program, funded by the Ministry of Trade, Industry and Energy (MOTIE) (N0001720).

References

1 L. Zhao, H. Wang, K. Huo, X. Zhang, W. Wang, Y. Zhang, Z. Wu and P. K. Chu, *Biomaterials*, 2013, **34**, 19–29.
2 T. U. Luu, S. C. Gott, B. W. Woo, M. P. Rao and W. F. Liu, *ACS Appl. Mater. Interfaces*, 2015, **7**, 28665–28672.
3 R. J. McMurray, N. Gadegaard, P. M. Tsimbouri, K. V. Burgess, L. E. McNamara, R. Tare, K. Murawski, E. Kingham, R. O. Oreffo and M. J. Dalby, *Nat. Mater.*, 2011, **10**, 637–644.
4 L. Y. Chan, W. R. Birch, E. K. Yim and A. B. Choo, *Biomaterials*, 2013, **34**, 382–392.
5 E. K. Yim, E. M. Darling, K. Kulangara, F. Guilak and K. W. Leong, *Biomaterials*, 2010, **31**, 1299–1306.
6 P. D. P. Dingal and D. E. Discher, *Nat. Mater.*, 2014, **13**, 532–537.
7 M. J. Dalby, N. Gadegaard and R. O. Oreffo, *Nat. Mater.*, 2014, **13**, 558–569.
8 K. K. Tan, J. Y. Tann, S. R. Sathe, S. H. Goh, D. Ma, E. L. Goh and E. K. Yim, *Biomaterials*, 2015, **43**, 32–43.
9 J. S. Chua, C. P. Chng, A. A. K. Moe, J. Y. Tann, E. L. Goh, K. H. Chiam and E. K. Yim, *Biomaterials*, 2014, **35**, 7750–7761.
10 K. Yang, K. Jung, E. Ko, J. Kim, K. I. Park, J. Kim and S. W. Cho, *ACS Appl. Mater. Interfaces*, 2013, **35**, 10529–10540.
11 Z. Pan, C. Yan, R. Peng, Y. Zhao, Y. He and J. Ding, *Biomaterials*, 2012, **33**, 1730–1735.
12 K. Yang, H. Jung, H. R. Lee, J. S. Lee, S. R. Kim, K. Y. Song, E. Cheong, J. Bang, S. G. Im and S. W. Cho, *ACS Nano*, 2014, **8**, 7809–7822.
13 L. E. McNamara, R. J. McMurray, M. J. Biggs, F. Kantawong, R. O. Oreffo and M. J. Dalby, *J. Tissue Eng.*, 2010, **1**, 120623.
14 G. Abagnale, M. Steger, V. H. Nguyen, N. Hersch, A. Sechi, S. Joussen, B. Denecke, R. Merkel, B. Hoffmann and A. Dreser, *Biomaterials*, 2015, **61**, 316–326.
15 M. J. Kim, B. Lee, K. Yang, J. Park, S. Jeon, S. H. Um, D. I. Kim, S. G. Im and S. W. Cho, *Biomaterials*, 2013, **34**, 7236–7246.
16 E. K. Yim, S. W. Pang and K. W. Leong, *Exp. Cell Res.*, 2007, **313**, 1820–1829.
17 K. Yang, E. Park, J. S. Lee, I. S. Kim, K. Hong, K. I. Park, S. W. Cho and H. S. Yang, *Macromol. Biosci.*, 2015, **15**, 1348–1356.
18 M. Yamada, K. Tanemura, S. Okada, A. Iwanami, M. Nakamura, H. Mizuno, M. Ozawa, R. Ohyama-Goto, N. Kitamura and M. Kawano, *Stem Cells*, 2007, **25**, 562–570.
19 N. C. Spitzer, *Nature*, 2006, **444**, 707–712.
20 F. Pires, Q. Ferreira, C. A. Rodrigues, J. Morgado and F. C. Ferreira, *Biochim. Biophys. Acta*, 2015, **1850**, 1158–1168.
21 O. Akhavan, E. Ghaderi, S. A. Shirazian and R. Rahighi, *Carbon*, 2016, **97**, 71–77.
22 G. Thrivikraman, G. Madras and B. Basu, *Biomaterials*, 2014, **35**, 6219–6235.
23 S. K. Seidlits, J. Y. Lee and C. E. Schmidt, *Nanomedicine*, 2008, **2**, 183–199.
24 J. Y. Lee, C. A. Bashur, A. S. Goldstein and C. E. Schmidt, *Biomaterials*, 2009, **30**, 4325–4335.

25 Y. J. Huang, H. C. Wu, N. H. Tai and T. W. Wang, *Small*, 2012, **8**, 2869–2877.
26 H. S. Yang, B. Lee, J. H. Tsui, J. Macadangdang, S. Y. Jang, S. G. Im and D. H. Kim, *Adv. Healthcare Mater.*, 2016, **5**, 137–145.
27 L. E. McNamara, T. Sjöström, K. E. Burgess, J. J. Kim, E. Liu, S. Gordonov, P. V. Moghe, R. D. Meek, R. O. Oreffo and B. Su, *Biomaterials*, 2011, **32**, 7403–7410.
28 M. Li, Y. Guo, Y. Wei, A. G. MacDiarmid and P. I. Lelkes, *Biomaterials*, 2006, **27**, 2705–2715.
29 K. Yang, J. S. Lee, J. Kim, Y. B. Lee, H. Shin, S. H. Um, J. B. Kim, K. I. Park, H. Lee and S. W. Cho, *Biomaterials*, 2012, **33**, 6952–6964.
30 E. Ko, K. Yang, J. Shin and S. W. Cho, *Biomacromolecules*, 2013, **14**, 3202–3213.
31 K. Yang, J. Lee, J. S. Lee, D. Kim, G. E. Chang, J. Seo, E. Cheong, T. Lee and S. W. Cho, *ACS Appl. Mater. Interfaces*, 2016, **8**, 1763–1774.
32 K. Yang, H. J. Park, S. Han, J. Lee, E. Ko, J. Kim, J. S. Lee, J. H. Yu, K. Y. Song, E. Cheong, S. R. Cho, S. Chung and S. W. Cho, *Biomaterials*, 2015, **63**, 177–188.
33 V. K. Balla, S. Bodhak, S. Bose and A. Bandyopadhyay, *Acta Biomater.*, 2010, **6**, 3349–3359.
34 D. Khang, J. Lu, C. Yao, K. M. Haberstroh and T. J. Webster, *Biomaterials*, 2008, **29**, 970–983.
35 M. Jones, I. McColl, D. Grant, K. Parker and T. Parker, *J. Biomed. Mater. Res.*, 2000, **52**, 413–421.
36 M. A. Shirazi, S. J. Marzo and J. P. Leonetti, *Otolaryngol.–Head Neck Surg.*, 2006, **134**, 236–239.
37 T. Kawase, S. Shibata, Y. Katori, A. Ohtsuka, G. Murakami and M. Fujimiya, *J. Anat.*, 2012, **221**, 331–340.
38 A. Akkouch, G. Shi, Z. Zhang and M. Rouabhia, *J. Biomed. Mater. Res., Part A*, 2010, **92**, 221–231.
39 A. S. Crouch, D. Miller, K. J. Luebke and W. Hu, *Biomaterials*, 2009, **30**, 1560–1567.
40 J. Lu, M. P. Rao, N. C. MacDonald, D. Khang and T. J. Webster, *Acta Biomater.*, 2008, **4**, 192–201.
41 G. Cellot, E. Cilia, S. Cipollone, V. Rancic, A. Sucapane, S. Giordani, L. Gambazzi, H. Markram, M. Grandolfo and D. Scaini, *Nat. Nanotechnol.*, 2009, **4**, 126–133.
42 C. E. Schmidt, V. R. Shastri, J. P. Vacanti and R. Langer, *Proc. Natl. Acad. Sci. U. S. A.*, 1997, **94**, 8948–8953.
43 V. Lovat, D. Pantarotto, L. Lagostena, B. Cacciari, M. Grandolfo, M. Righi, G. Spalluto, M. Prato and L. Ballerini, *Nano Lett.*, 2005, **5**, 1107–1110.
44 Y. Yang, R. Glover and J. L. Ong, *Colloids Surf., B*, 2003, **30**, 291–297.
45 M. J. Dalby, N. Gadegaard, R. Tare, A. Andar, M. O. Riehle, P. Herzyk, C. D. Wilkinson and R. O. Oreffo, *Nat. Mater.*, 2007, **6**, 997–1003.
46 M. J. P. Biggs, R. G. Richards and M. J. Dalby, *Nanomed. Nanotechnol. Biol. Med.*, 2010, **6**, 619–633.
47 J. D. Foley, E. W. Grunwald, P. F. Nealey and C. J. Murphy, *Biomaterials*, 2005, **26**, 3639–3644.
48 A. Hamadi, M. Bouali, M. Dontenwill, H. Stoeckel, K. Takeda and P. Rondé, *J. Cell Sci.*, 2005, **118**, 4415–4425.
49 R. Zaidel-Bar, R. Milo, Z. Kam and B. Geiger, *J. Cell Sci.*, 2007, **120**, 137–148.
50 S. Woo and T. M. Gomez, *J. Neurosci.*, 2006, **26**, 1418–1428.
51 M. Santiago-Medina, K. A. Gregus and T. M. Gomez, *J. Cell Sci.*, 2013, **126**, 1122–1133.
52 J. P. Myers, M. Santiago-Medina and T. M. Gomez, *Dev. Neurobiol.*, 2011, **71**, 901–923.
53 P. C. Kerstein, I. Nichol and T. M. Gomez, *Front. Cell. Neurosci.*, 2015, **9**, 244.
54 C. Schulte, S. Rodighiero, M. A. Cappelluti, L. Puricelli, E. Maffioli, F. Borghi, A. Negri, E. Sogne, M. Galluzzi and C. Piazzoni, *J. Nanobiotechnol.*, 2016, **14**, 18.
55 Y. C. Chen, D. C. Lee, T. Y. Tsai, C. Y. Hsiao, J. W. Liu, C. Y. Kao, H. K. Lin, H. C. Chen, T. J. Palathinkal and W. F. Pong, *Biomaterials*, 2010, **31**, 5575–5587.
56 I. Ivankovic-Dikic, E. Grönroos, A. Blaukat, B. U. Barth and I. Dikic, *Nat. Cell Biol.*, 2000, **2**, 574–581.
57 C. H. Seo, K. Furukawa, K. Montagne, H. Jeong and T. Ushida, *Biomaterials*, 2011, **32**, 9568–9575.
58 B. K. K. Teo, S. T. Wong, C. K. Lim, T. Y. Kung, C. H. Yap, Y. Ramagopal, L. H. Romer and E. K. Yim, *ACS Nano*, 2013, **7**, 4785–4798.
59 K. Nakamura, H. Yano, H. Uchida, S. Hashimoto, E. Schaefer and H. Sabe, *J. Biol. Chem.*, 2000, **275**, 27155–27164.
60 C. E. Turner, *Nat. Cell Biol.*, 2000, **2**, E231–E236.
61 A. M. Pasapera, I. C. Schneider, E. Rericha, D. D. Schlaepfer and C. M. Waterman, *J. Cell Biol.*, 2010, **188**, 877–890.
62 S. Watari, K. Hayashi, J. A. Wood, P. Russell, P. F. Nealey, C. J. Murphy and D. C. Genetos, *Biomaterials*, 2012, **33**, 128–136.
63 C. J. Bettinger, R. Langer and J. T. Borenstein, *Angew. Chem., Int. Ed.*, 2009, **48**, 5406–5415.
64 E. Den Braber, J. De Ruijter, L. Ginsel, A. Von Recum and J. Jansen, *J. Biomed. Mater. Res.*, 1998, **40**, 291–300.
65 J. Xie, S. M. Willerth, X. Li, M. R. Macewan, A. Rader, S. E. Sakiyama-Elbert and Y. Xia, *Biomaterials*, 2009, **30**, 354–362.
66 W. Song, D. An, D. I. Kao, Y. C. Lu, G. Dai, S. Chen and M. Ma, *ACS Appl. Mater. Interfaces*, 2014, **6**, 7038–7044.
67 M. T. Frey, I. Y. Tsai, T. P. Russell, S. K. Hanks and Y. l. Wang, *Biophys. J.*, 2006, **90**, 3774–3782.
68 R. O. Hynes, *Cell*, 1992, **69**, 11–25.
69 B. K. K. Teo, S. Ankam, L. Y. Chan and E. K. Yim, *Methods Cell Biol.*, 2010, **98**, 241–294.
70 C. H. Seo, H. Jeong, K. S. Furukawa, Y. Suzuki and T. Ushida, *Biomaterials*, 2013, **34**, 1764–1771.
71 K. Abe and H. Saito, *Neurosci. Res.*, 2000, **36**, 251–257.
72 S. L. Fyffe-Maricich, J. C. Karlo, G. E. Landreth and R. H. Miller, *J. Neurosci.*, 2011, **31**, 843–850.
73 J. W. Mandell, N. C. Gocan and S. R. Vandenberg, *Glia*, 2001, **34**, 283–295.
74 K. Riento and A. J. Ridley, *Nat. Rev. Mol. Cell Biol.*, 2003, **4**, 446–456.

75 F. Matsumura, *Trends Cell Biol.*, 2005, **15**, 371–377.
76 S. Sonam, S. R. Sathe, E. K. Yim, M. P. Sheetz and C. T. Lim, *Sci. Rep.*, 2016, **6**, 20415.
77 S. Ankam, C. K. Lim and E. K. Yim, *Biomaterials*, 2015, **47**, 20–28.
78 S. Mruthyunjaya, R. Manchanda, R. Godbole, R. Pujari, A. Shiras and P. Shastry, *Biochem. Biophys. Res. Commun.*, 2010, **391**, 43–48.
79 K. M. Kollins, R. L. Bell, M. Butts and G. S. Withers, *Neural Dev.*, 2009, **4**, 26.
80 K. Kim, O. Ossipova and S. Y. Sokol, *Stem Cells*, 2015, **33**, 674–685.
81 Y. Kamishibahara, H. Kawaguchi and N. Shimizu, *Neurosci. Lett.*, 2016, **615**, 44–49.
82 X. F. Jia, F. Ye, Y. B. Wang and D. X. Feng, *Neural Regener. Res.*, 2016, **11**, 983–987.
83 A. A. K. Moe, M. Suryana, G. Marcy, S. K. Lim, S. Ankam, J. Z. W. Goh, J. Jin, B. K. K. Teo, J. B. K. Law and H. Y. Low, *Small*, 2012, **8**, 3050–3061.
84 C. Strübing, G. Ahnert-Hilger, J. Shan, B. Wiedenmann, J. Hescheler and A. M. Wobus, *Mech. Dev.*, 995, **53**, 275–287.
85 J. Mariani, G. Coppola, P. Zhang, A. Abyzov, L. Provini, L. Tomasini, M. Amenduni, A. Szekely, D. Palejev and M. Wilson, *Cell*, 2015, **162**, 375–390.
86 R. Gao and P. Penzes, *Curr. Mol. Med.*, 2015, **15**, 146–167.
87 Y. Jin, J. Seo, J. S. Lee, S. Shin, H. J. Park, S. Min, E. Cheong, T. Lee and S. W. Cho, *Adv. Mater.*, 2016, **28**, 7365–7374.
88 L. Song, K. Wang, Y. Li and Y. Yang, *Colloids Surf., B*, 2016, **148**, 49–58.
89 E. Stewart, N. R. Kobayashi, M. J. Higgins, A. F. Quigley, S. Jamali, S. E. Moulton, R. M. Kapsa, G. G. Wallace and J. M. Crook, *Tissue Eng., Part C*, 2014, **21**, 385–393.
90 D. A. Balikov, B. Fang, Y. W. Chun, S. W. Crowder, D. Prasai, J. B. Lee, K. I. Bolotin and H. J. Sung, *Nanoscale*, 2016, **8**, 13730–13739.